

Giant resonance structure in ^{208}Pb measured using the (p,p') reaction at 334 MeV

F. E. Bertrand, E. E. Gross, D. J. Horen, R. O. Sayer, and T. P. Sjoreen
Oak Ridge National Laboratory, Oak Ridge, Tennessee 37831

D. K. McDaniels, J. Lisantti, and J. R. Tinsley
University of Oregon, Eugene, Oregon 97403

L. W. Swenson
Oregon State University, Corvallis, Oregon 97330

J. B. McClelland, T. A. Carey, K. Jones, and S. J. Seestrom-Morris
Los Alamos National Laboratory, Los Alamos, New Mexico 98545

(Received 8 May 1985)

The structure of giant resonances in ^{208}Pb has been studied using inelastic scattering of 334-MeV polarized protons. Data were obtained with 70-keV energy resolution over an angular range from 2–13 deg and the spectra were measured over an excitation energy range from 0–25 MeV. The results show that the quadrupole resonance strength is divided into two main components, one centered at 10.6 MeV containing 70% of the energy-weighted sum rule in a 2-MeV wide peak and a second component composed of several discrete peaks located between 7 and 9 MeV which deplete a total of approximately 20% of the energy-weighted sum rule. The giant monopole and dipole resonances as well as a hexadecapole resonance are observed. Measurements of differential cross sections for elastic scattering and inelastic scattering to low-lying 3^- , 2^+ , and 4^+ levels are presented. Comparison of these data with collective model direct reaction calculations shows the calculations to correctly describe the shape and magnitude of the cross sections when normalized to the known transition rates for each level.

I. INTRODUCTION

Over the past ten years giant multipole resonances in ^{208}Pb have been studied¹ with a wide variety of hadronic and electromagnetic probes. A large number of giant resonances, including the isoscalar and isovector giant quadrupole resonance (GQR), the isoscalar and isovector giant monopole resonance (GMR), a $2\hbar\omega$ giant hexadecapole resonance (GHR), and the $3\hbar\omega$ isoscalar giant octupole resonance (GOR) have been located. There is generally excellent agreement among the various hadron reactions as to the location, angular momentum, and strength (sum rule depletion) of the resonances in ^{208}Pb . However, there exist substantial differences between hadron and electron scattering measurements. In particular, high energy resolution electron scattering measurements² using 30-, 40-, and 50-MeV electrons indicate that the quadrupole resonance is fragmented into a very large number of peaks (> 60) with a total cross section which depletes 29% (+11, -8%) of the $L=2$, energy weighted sum rule (EWSR). Hadron measurements show the existence of a concentration of quadrupole strength near 11 MeV which depletes most of the EWSR.

There are two features of the electron scattering work of Ref. 2 that may contribute to the differences with hadron measurements. First, the energy resolution of the electron measurements is better than that commonly obtained in hadron inelastic scattering. Second, the energy of the electrons used in the work of Ref. 2 is low enough

to exclude the excitation of $L > 2$ giant resonances. Such exclusion is generally not the case in the hadron measurements. For example, in the case of the (α, α') reaction the angular distribution for $L=4$, and $L=2$ momentum transfers are, except at very small angles, nearly identical leading to the possibility that any hexadecapole strength in the GQR region could obscure the quadrupole resonance fine structure reported in Ref. 2.

In order to provide a careful study of the hadron excitation of giant resonance structure near the GQR region in ^{208}Pb and in particular to provide a comparison with results from the electron scattering work we have measured the reaction $^{208}\text{Pb}(p,p')$ using 334-MeV polarized protons. Earlier giant resonance studies using the $^{208}\text{Pb}(p,p')$ reaction included measurements with a 45 MeV beam³ and with a 201 MeV beam.⁴ The measurements reported in the present work were performed with an energy resolution of 70 keV, comparable to that in the electron scattering measurements of Ref. 2 and in the medium energy proton scattering measurements of Ref. 4, and considerably better than that obtained in most previous hadron experiments. Although the 45 MeV (p,p') data were measured with even better energy resolution, that experiment was performed at an incident energy too low to provide clear excitation of the giant resonance states. An important feature relevant to the use of medium-energy proton inelastic scattering is the good selectivity to momentum transfer. This feature is illustrated in Fig. 1 which shows distorted-wave Born approximation (DWBA) calculations

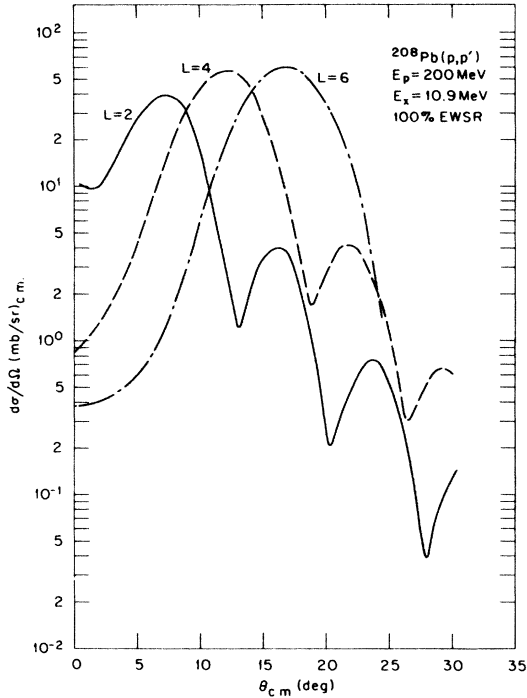


FIG. 1. Calculated angular distributions for 200-MeV proton inelastic scattering to 2^+ , 4^+ , and 6^+ states at 10.9 MeV in ^{208}Pb . The calculations are normalized to 100% depletion of the respective energy weighted sum rules.

for 200-MeV proton inelastic scattering on ^{208}Pb for states at 10.9 MeV that exhaust 100% of their respective EWSR's. The angular distributions for the various L transfers peak at considerably different angles. This feature of medium energy proton inelastic scattering allows more certain identification of resonance multipolarity. Furthermore, it provides confidence that spectra measured at an angle of maximum quadrupole strength will contain little contribution from resonances with neighboring angular momentum.

An experiment by Djalali *et al.*⁴ has utilized these features of medium energy proton inelastic scattering to study the giant resonance structure in ^{208}Pb with 201 MeV protons. That experiment reported an energy weighted sum rule depletion of $24 \pm 3\%$ for the isoscalar giant quadrupole resonance. As mentioned above this value is about three times smaller than has been reported¹ in nearly every other hadron inelastic scattering study of giant resonances. It is important to note that the authors of Ref. 4 point out that their analysis of the excitation of the well-known low-lying states in ^{208}Pb yields values for the transition rates to those states that are a factor of 2 lower than accepted values.

The present data provide a very high resolution measurement of giant resonance structure in ^{208}Pb using a probe that strongly excites the resonances and that provides momentum transfer selectivity over a wide angle range. We believe that our data remove the objections to comparisons of previous hadron data with the electron

scattering results. Furthermore, we believe it is important to independently determine whether the low EWSR values reported in Ref. 4 using 201 MeV protons are correct.

Our data also provide high resolution measurements of the differential cross sections and analyzing powers for elastic scattering and for inelastic excitation of some low-lying states in ^{208}Pb . To obtain optical model parameters for the DWBA calculations used to analyze the inelastic scattering angular distributions, we have performed an extensive analysis of previously reported⁵ ^{208}Pb elastic scattering data for 200-, 300-, and 400-MeV polarized protons including both differential cross sections and analyzing powers.

II. EXPERIMENT

Giant resonance spectra were obtained by measuring inelastic scattering of 334-MeV polarized protons from the Clinton P. Anderson Meson Physics Facility (LAMPF) of the Los Alamos National Laboratory from a ^{208}Pb target. The polarization direction of the proton beam was perpendicular to the reaction plane. The beam polarization was periodically determined by measuring the proton scattering from a hydrogenous target located upstream from the scattering chamber. The average beam polarization during the course of the experiment was measured to be $|0.83 \pm 0.02|$.

Inelastically scattered protons were detected with the high resolution spectrograph (HRS) using the standard focal plane detector system. The angular acceptance of the spectrograph was about 1.8 deg and the usable energy acceptance was approximately four percent. Since no beam current integration is available at small angles, absolute cross sections were determined by normalization of our measurement of proton-proton scattering on a CH_2 target to accepted cross section values.⁶ Relative beam intensity was monitored by two ion chambers placed in the beam near the exit of the scattering chamber. At the smallest scattering angle, 2.75 deg, it was not possible to use the in-beam ion chambers because they produced scattering into the focal plane of the magnetic spectrometer. Absolute cross sections were obtained for the 2.75-deg data by overlapping the data with a run taken at 3.75 deg where the ion chambers could be used without affecting the spectra. We estimate the uncertainty in the absolute normalization to be $\pm 8\%$.

Considerable care was taken to ensure that the spectra, particularly at small angles and at high-excitation energies, were not compromised by background. Measurements were made at all angles using a blank target frame, and the beam could always be tuned so as to eliminate all background. We have also checked the beam quality (i.e., lower energy components) by measuring the spectrum from ^{48}Ca at the smallest angles. At 2–4 deg, the ^{48}Ca spectrum is so dominated by excitation of the 10.28-MeV, 1^+ state that any “bogus” background near 10 MeV should be easily observable at the level of a few parts in 10^3 . In our measurements we observe this state with very little background which indicates the “cleanliness” of our ^{208}Pb spectra in the same excitation energy region. The achievement of this spectral “cleanliness” was facilitated

by the use of the many available “cuts” on the focal plane data from the HRS. The same cuts used for the small angle giant resonance spectra were also used for the normalization runs.

Due to the small momentum acceptance of the HRS, spectra were obtained for two settings of the magnetic field for each angle. In this way data covering an excitation energy range of 0–25 MeV were obtained. Measurements were made at central angles of 2.75, 3.75, 5.75, 7.75, 9.75, and 12.75 deg. The data were then analyzed in two 0.8 deg angle bins for each run. The efficiency of the HRS detector system as a function of focal plane position was determined by moving a peak from elastic scattering from a lead target across the focal plane at a fixed angle. The efficiency of the detector system decreased at the high and low excitation energy extremes by less than 6% for the focal plane region utilized in these measurements. During the latter part of the experiment a wire in the focal plane detector became faulty so that the focal plane efficiency at the position of this wire was greatly reduced resulting in an approximately 400 keV wide gap or “glitch” near 16 and 22 MeV in the excitation energy spectra of the larger angle data. The data at angles $\leq 5.25^\circ$ were obtained prior to breakdown of the wire in the detector system. The peak-fitting program used to analyze the spectra includes an option to omit one or more groups of data channels within the fitting region from the chi-squared minimization search. Peaks in the large angle spectra were fitted using the omit feature of the peak-fitting program to minimize the effect of the faulty wires on the spectrum analysis. The spectra shown in the paper have not been corrected for the glitch caused by the faulty wire or for the loss of focal plane efficiency of $\sim 6\%$ at each end of the focal plane region used in this experiment. The cross sections have, however, been corrected for both of these problems. The ^{208}Pb target was a self-supporting rolled foil of isotopically enriched material having a thickness of 56 mg/cm^2 . The CH_2 target had a thickness of 23.1 mg/cm^2 .

III. EXPERIMENTAL RESULTS

A typical spectrum for ^{208}Pb is shown in Fig. 2. The peaks from elastic scattering and from excitation of the $2.61 \text{ MeV}, 3^-$ state are not shown. The spectrum is for 7.25° and is plotted using two different vertical scales. The energy resolution in this, and all other spectra, is approximately 70 keV. There are several interesting features to point out at excitation energies above 7 MeV. It is clear that a broad peak is seen near 10.5 MeV, in agreement with other hadron measurements for the GQR.¹ However, at lower excitation energies (7–10 MeV) we find several discrete states having widths of about 400 keV that are observed at all angles. There is a very prominent peak located at $\sim 13.6 \text{ MeV}$. The well-known giant dipole resonance (GDR) and the giant monopole resonance (GMR) are located near this excitation energy. The dip in some of the spectra near 16 and 22 MeV of excitation energy was caused by a faulty wire in the focal plane detector system and was discussed above.

Figure 3 shows spectra from ^{208}Pb at 7.25° for spin

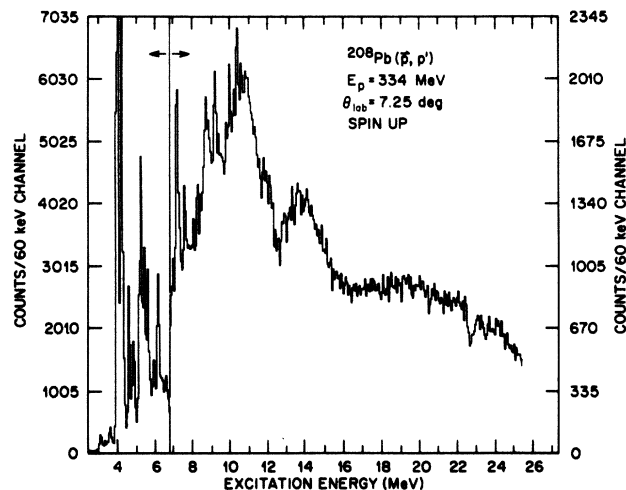


FIG. 2. Inelastic scattering spectrum from ^{208}Pb at 7.25° . Note the scale change near 7 MeV.

up and spin down incident protons. The two spectra are plotted on the same relative cross section scale. For all of the inelastic excitations we have studied in this work, the spin-down cross sections are smaller than or equal to the spin-up cross sections. Although we later show the quantitative analyzing power for these peaks, we find the measurement of the analyzing power for the giant resonances does not add greatly to our knowledge of these resonances.

Figure 4 shows inelastic spectra at several angles for an excitation energy range of 6–25 MeV and also indicates the manner in which the spectra were analyzed. The vertical scale for the plots does not begin at zero in all cases. The smooth solid curves are fits to the observed peaks.

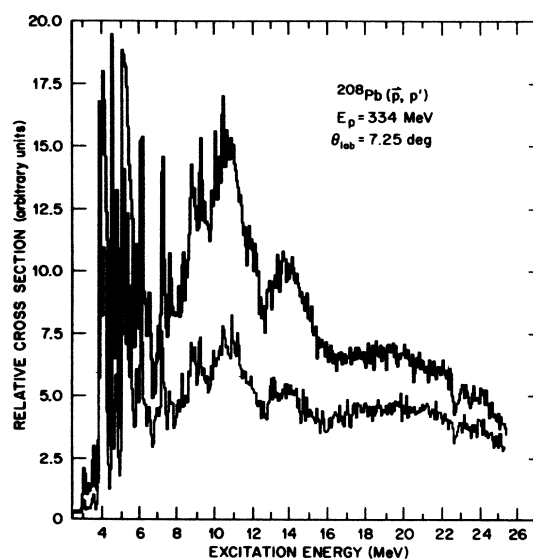


FIG. 3. Inelastic scattering spectra from ^{208}Pb at 7.25° . The dark curve is the spectrum from inelastic scattering of spin up protons and the lighter curve is from scattering of spin down protons. The two spectra are plotted on the same relative cross section scale.

We have fitted the “GDR” peak with energy and width taken from photonuclear measurements.⁷ We have used a Gaussian peak shape for all the other analyzed peaks. Due to the inherently high uncertainty associated with the extraction of giant resonance peak shapes, there is no real evidence to suggest that a Lorentzian shape is to be preferred over a Gaussian shape. Within the large uncertainties in the cross sections we do not believe that the choice of the two shapes matters. The generally flat horizontal curve is the assumed shape of the nuclear continuum underlying the giant resonance peaks. This “background” was established by connecting a smooth curve to the spectra at high excitation energy where no resonance peaks are visible to a point at the low excitation end of the spectra where discrete states can be seen. The points in between these two extremes are drawn by the authors to follow their concept of the continuum shape. We have also analyzed the data by using a procedure in which the continuum background is described as a Gaussian at excitation energies below quasifree scattering and above that point the continuum is described by a fourth order polynomial drawn through the data. From the effect of these two different techniques on the resonance cross sections and from our past experience we assign a minimum un-

certainty of $\pm 20\%$ to the giant resonance cross sections. The uncertainty in this process is, of course, rather large and is the dominant uncertainty associated with the process of extracting giant resonance cross sections. No theoretical calculation is available that adequately describes both the shape and magnitude of the inelastic continuum over the angle range covered in this experiment.

At the smallest angles, the spectra are dominated by the peak at ~ 13.6 MeV of excitation energy. Since the GDR is located at 13.6 MeV in ^{208}Pb , and as we discuss later, the GDR is strongly Coulomb excited at small angles, we assume the peak we observe for $\theta_{\text{lab}} < 5$ deg arises from GDR excitation. We do not believe that we can separate the peak in our spectra near 13.6 MeV into separate GMR and GDR contributions. Our calculations indicate that for angles larger than ~ 5 deg the excitation of the GMR located at 13.9 MeV becomes dominant over the GDR excitation. For this reason, for angles larger than five degrees we fit the spectra with a peak having the known¹⁶ energy, 13.9 MeV, and width, 2.8 MeV, of the GMR. There is some evidence in the spectra that the ~ 13.6 MeV peak shifts toward higher excitation energies for larger angles of observation.

By 4.25 deg, the spectra are dominated by a peak locat-

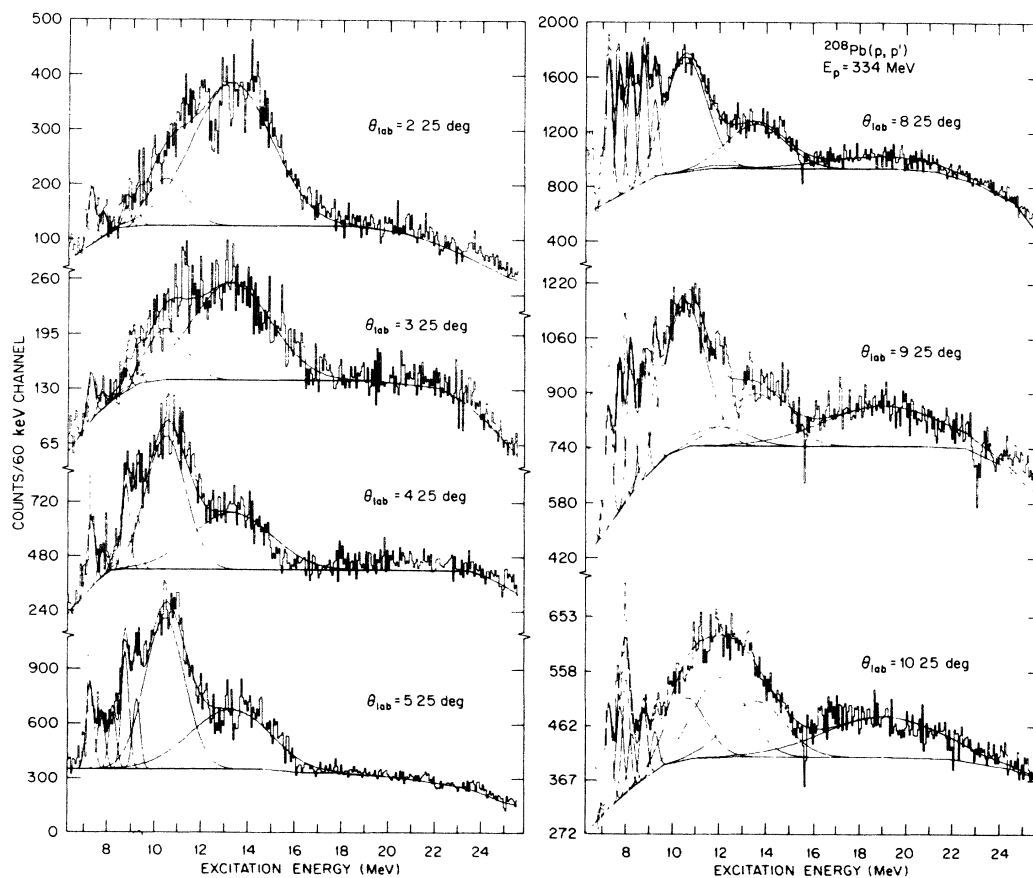


FIG. 4. Inelastic proton scattering spectra for several angles of observation. The data are plotted beginning at 7 MeV of excitation energy. The vertical scale is usually not plotted from zero. The data are the histogram curve. The solid curves on the plots for each angle are the fits to the data. The generally horizontal solid curve on each spectrum is the author's estimate of the shape and magnitude of the nuclear continuum underlying the giant resonance peaks. The Gaussian curves are peak fits to the various giant resonances described in the text.

ed at 10.6 MeV and by several narrow peaks at lower excitation energies. The narrow peaks have excitation energies of 7.36, 7.84, 8.11, 8.35, 8.86, and 9.34 MeV. It should be noted that the spectrum decomposition shown in Fig. 4 seems to show only five narrow peaks at some angles. This is due to the fact that the cross section for the 8.11 meV peak is very small at forward angles compared to the cross section for the nearby 8.35 MeV peak. Because of this the 8.11 MeV peak is not always visible in the figures although the peak is always included in the drawing. On the other hand, both the 8.11 and 8.35 MeV peaks are visible at the larger angles where the cross sections for the two peaks are more comparable.

For $\theta_L \gtrsim 8.25$ deg our spectra show the existence of a broad peak centered at about 19 MeV of excitation energy, the energy¹ of the $3\hbar\omega$ component of the giant octupole resonance (GOR). We cannot establish an accurate cross section for the GOR since the resonance is very broad (~ 6 MeV) and our data do not extend to high enough excitation energy. For the purpose of this paper we assume the existence of the GOR from previous data.

The 9.25- and the 10.25-deg spectra (Fig. 4) no longer show two peaks located at 10.6 and 13.6 MeV. Rather, the larger angle spectra show a single broad peak located at ~ 12 MeV. As shown in Fig. 5(a), this broad peak cannot be fitted using only the parameters for GQR and GMR peaks that provided fits to the smaller angle spectra. However, as shown in Fig. 5(b), if, as we have previously reported,⁸ we assume there is another peak located

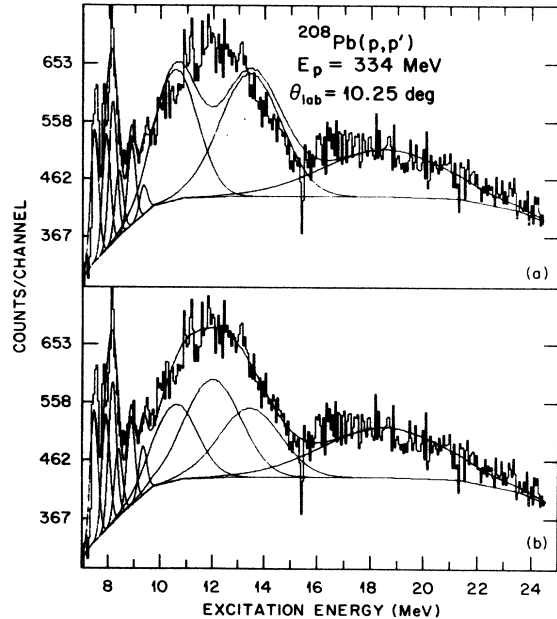


FIG. 5. Inelastic proton spectrum from ^{208}Pb at 10.25 deg. (a) Spectrum is fitted with an assumed continuum shape (horizontal solid curve) and with the same giant resonance peaks (and same parameters for those peaks) as used at smaller angles. The fit to the spectrum is noticeably poor in the region of 12 MeV of excitation energy. (b) Spectrum is fitted with the same continuum as in (a) and with the same peaks except that a peak is included at 12.0 MeV having a width of 2.4 MeV.

TABLE I. Properties of observed continuum peaks.

Excitation energy (MeV)	Width FWHM (MeV)	L	EWSR fraction (%)
7.36(0.05)	0.4(0.05)	2	6.5 (1)
7.84(0.05)	0.4(0.05)	2	4.2 (0.6)
8.11(0.05)	0.4(0.05)	4	3 (1.5)
8.35(0.05)	0.4(0.05)	3	4 (1.2)
8.86(0.05)	0.4(0.05)	2	7 (1)
9.34(0.05)	0.4(0.05)	2	5 (0.8)
10.6 (0.2)	2.0(0.20)	2	70 (14)
12.0 (0.3)	2.4(0.2)	4	10 (3)
13.6 ^a	4.0	1	100
12.9 ^a	2.9	0	100

^aParameters assumed from previous measurements. GDR parameters used for $\theta_{\text{lab}} < 5^\circ$, GMR parameters used for $\theta_{\text{lab}} > 5^\circ$.

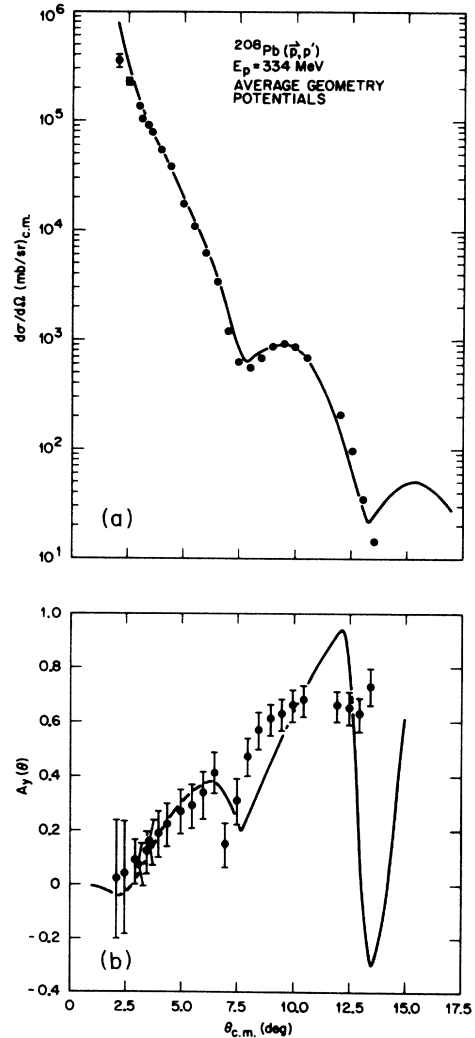


FIG. 6. Experimental and calculated elastic scattering differential cross sections and analyzing powers for 334-MeV protons on ^{208}Pb .

at 12 MeV, we are able to fit the large angle spectra. The results of this fit indicate the existence of a peak at 12.0 MeV having width of 2.4 MeV. This peak is certainly the same peak we previously assigned⁸ as a $2\hbar\omega$, hexadecapole resonance.

Table I provides a list of the peaks we have fitted to the spectra for excitation energies above 7 MeV. The energies and widths for the GDR and GMR are those deduced

from other work since in the present work we could not separate the two resonances.

Cross sections and analyzing powers for elastic scattering and for inelastic scattering to the 2.613-MeV, 3^- , 4.086-MeV, 2^+ , and 4.324-MeV, 4^+ , levels in ^{208}Pb are shown in Figs. 6, 7, and 8. Figure 9 shows the measured angular distribution and analyzing power for the 10.6-MeV peak. The differential cross sections for the narrow peaks located between 7 and 10 MeV are in Fig. 10, while Figs. 11 and 12 show the differential cross sections for the 13.6-MeV peak and the 12.0-MeV peak, respectively. The uncertainties in the giant resonance cross sections are dominated by the uncertainty in the shape and magnitude assumed for the nuclear continuum underlying the giant resonance peaks. In general, the uncertainties in the resonance cross sections are not less than 20%. The uncertainties in the values of the analyzing powers are usually dominated by statistics and not by uncertainty in the value of the beam polarization. The solid and dashed curves in Figs. 6–12 are from calculations that are described in the following sections.

IV. ANALYSIS

A. Elastic scattering

The elastic scattering differential cross sections and analyzing powers measured at 334 MeV (Fig. 6) were not extensive enough to determine the 12 parameters of the

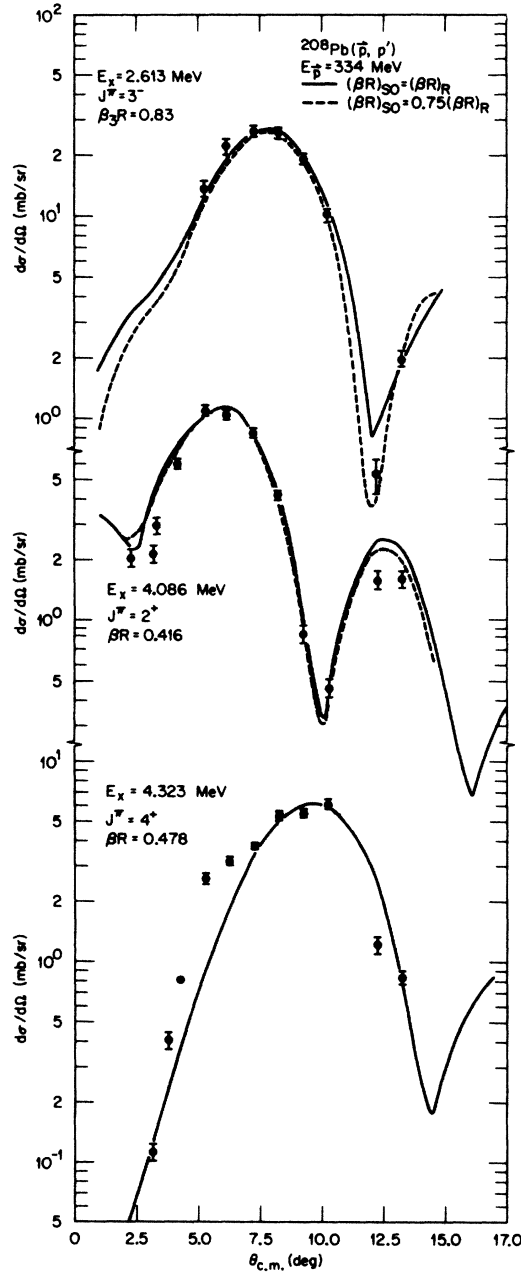


FIG. 7. Measured and calculated differential cross sections for excitation of three low-lying states in ^{208}Pb by inelastic scattering of 334-MeV polarized protons. The solid curve is from the DWBA calculation using the real potential deformation length equal to the spin-orbit potential deformation length. The dashed curve is the same calculation using the spin-orbit potential deformation length equal to 0.75 of the real potential deformation length.

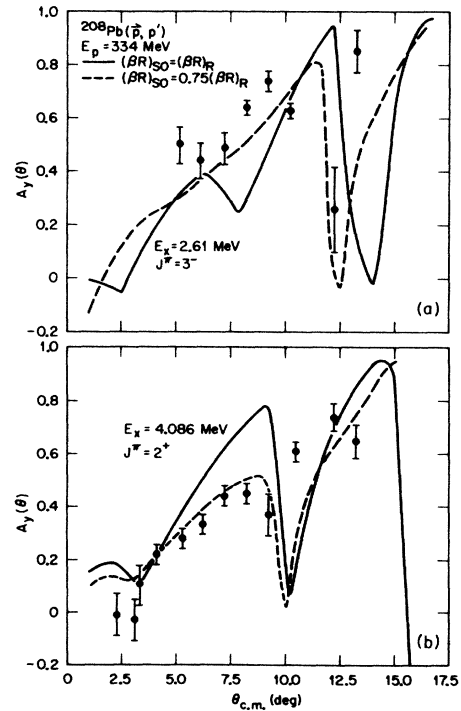


FIG. 8. Measured and calculated analyzing powers for excitation of the 2.613-MeV, 3^- state and the 4.086-MeV, 2^+ state in ^{208}Pb by 334-MeV polarized protons. The solid and dashed curves have the same meaning as in Fig. 7.

optical potential. Use of potentials developed from lower energy data was believed to be unreliable. Therefore, we analyzed very extensive cross section and polarization data for 200-, 300-, and 400-MeV proton elastic scattering from ^{208}Pb reported by Hutcheon.⁵ As a starting point for the analysis, we used the optical potential systematics

$$V(r) = V_c(r) - V_0 \left[\frac{1}{e^{x_0} + 1} \right] - iW \left[\frac{1}{e^{x'} + 1} \right] + \left[\frac{\hbar}{m_{\pi}c} \right]^2 V_s \frac{1}{r} \frac{d}{dr} \left[\frac{1}{e^{x_s} + 1} \right] \sigma \cdot \mathbf{l} + i \left[\frac{\hbar}{m_{\pi}c} \right]^2 W_s \frac{1}{r} \frac{d}{dr} \left[\frac{1}{e^{x'_s} + 1} \right] \sigma \cdot \mathbf{l}. \quad (1)$$

In this expression $V_c(r)$ is the Coulomb potential for a uniformly charged sphere of radius $1.2A^{1/3}$ fm, V_0 is the real potential, W is the imaginary volume potential, and V_s and W_s are the real and imaginary strengths of the spin orbit potential. The remaining factors contain the

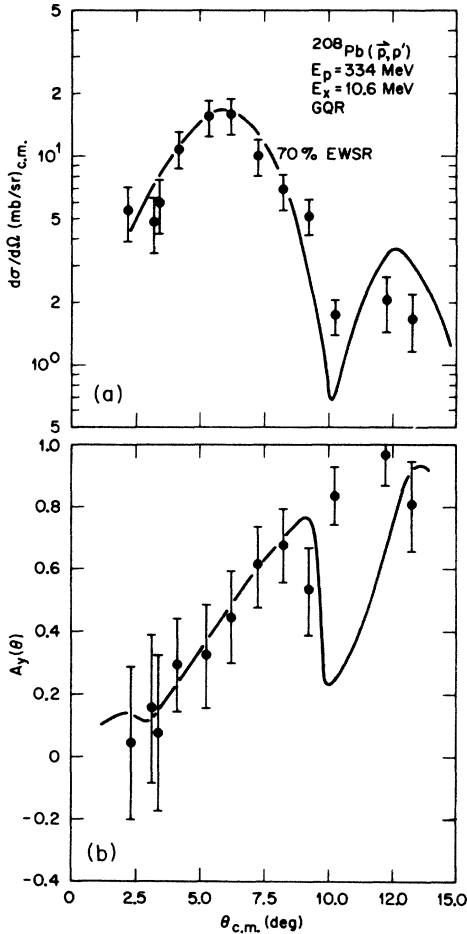


FIG. 9. Measured and calculated differential cross sections for the giant resonance peak located at 13.6 MeV in ^{208}Pb . The peak is interpreted as arising from excitation of both the GDR and the GMR. The solid curve is a calculation for excitation of the GDR using both nuclear and Coulomb potentials. The dashed curve is the calculated cross section for excitation of the GMR. The calculations for both of the giant resonances are normalized to 100% depletion of the respective EWSR's.

of Nadasen *et al.*⁹ for proton energies ≤ 180 MeV and searched on each set of data using the automatic search routine in the computer program ECIS (Ref. 10) which provides for relativistic effects in the scattering.

A 12 parameter optical potential was employed of the following form:

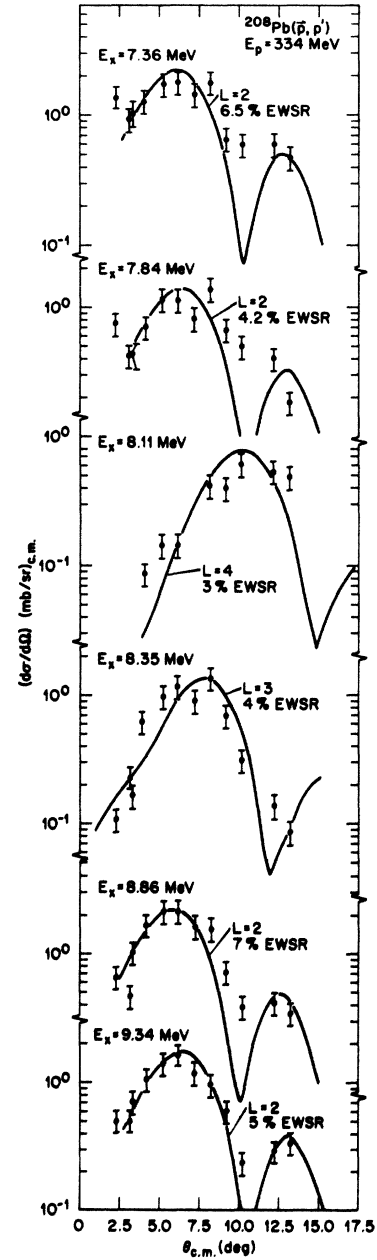


FIG. 10. Measured and calculated differential cross sections and analyzing powers for the giant resonance peak located at 10.6 MeV which is interpreted as the GQR.

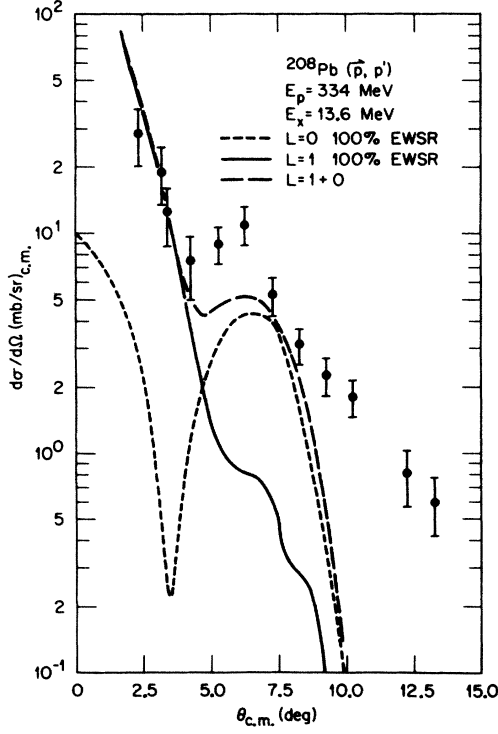


FIG. 11. Measured and calculated differential cross sections for excitation of seven peaks located at excitation energies above the neutron threshold but below the GQR. The calculated angular distributions are shown only for the L transfer that best fits the experimental data. The EWSR values shown are deduced from normalization of the calculated cross section to the measured cross section as detailed in the text.

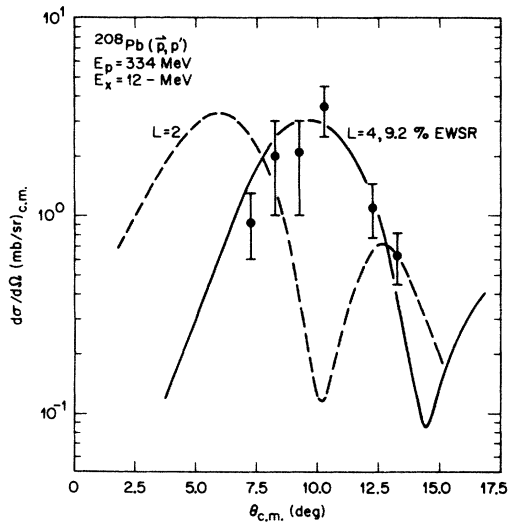


FIG. 12. Measured and calculated differential cross sections for excitation of a peak observed at 12.0 MeV. The solid curve is the calculation for $L=4$ transfer and the dashed curve is for $L=2$.

TABLE II. Proton plus ^{208}Pb optical parameters.

	334 MeV		200 MeV		300 MeV		400 MeV	
	Average geometry	Fit	Average geometry	Fit	Average geometry	Fit	Average geometry	Fit
V_0 (MeV)	4.452	12.46	11.17	11.11	4.37	4.934	0.292	0.20
r_0 (fm)	1.315	1.121	1.315	1.299	1.315	1.304	1.315	1.341
a_0 (fm)	0.599	0.770	0.599	0.623	0.599	0.606	0.599	0.568
W' (MeV)	21.65	30.00	21.17	20.38	25.19	24.48	34.12	33.49
r' (fm)	1.149	1.090	1.149	1.167	1.149	1.165	1.149	1.116
a' (fm)	0.799	0.765	0.799	0.827	0.799	0.762	0.799	0.808
V_s (MeV)	2.11	1.89	2.20	2.65	2.32	2.105	2.211	2.230
r_s (fm)	1.104	1.138	1.104	1.095	1.104	1.098	1.104	1.120
a_0 (fm)	0.689	0.777	0.689	0.685	0.689	0.651	0.689	0.730
W'_s (MeV)	-0.528	-0.770	-2.859	-2.88	-3.24	-3.314	-4.894	-3.630
r'_s (fm)	1.061	1.135	1.061	1.050	1.061	1.058	1.061	1.076
a'_s (fm)	0.801	0.687	0.801	0.821	0.801	0.785	0.801	0.799
χ^2_σ	956	554	3710	1670	1530	2110	1580	1040
χ^2_A	644	246	1820	2000	663	820	4150	3030

Woods-Saxon radius and diffusivity parameters: $x_0 = (r - R_0)/a_0$, $x' = (r - R')/a'$, $x_s = (r - R_s)/a_s$, $x'_s = (r - R'_s)/a'_s$, $R_0 = r_0 A^{1/3}$, $R' = r' A^{1/3}$, $R_s = r_s A^{1/3}$, $R'_s = r'_s A^{1/3}$; m_π is the pion rest mass.

The best fit parameters are summarized in Table II and the fits to the 200-, 300-, and 400-MeV elastic cross sections and polarizations are shown in Figs. 13 and 14, respectively. The fits to the differential cross sections are

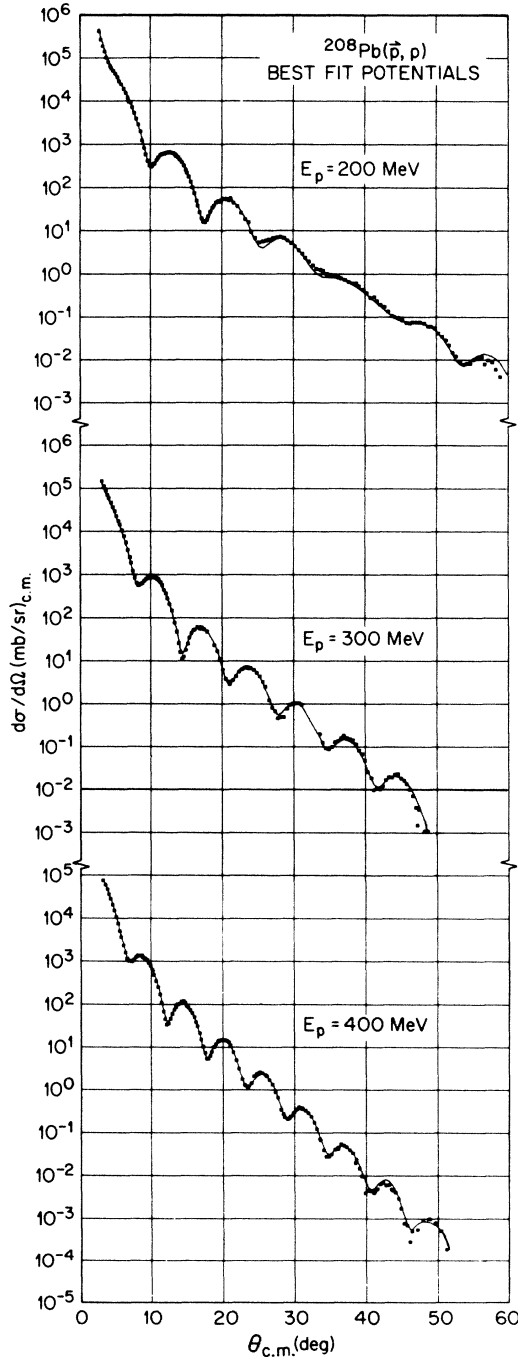


FIG. 13. Measured and calculated differential cross sections for elastic scattering of 200-, 300-, and 400-MeV protons by ^{208}Pb . The data are from Ref. 5 and the calculations performed by the present authors are discussed in the text.

generally excellent for $200 \leq E_p \leq 400$ MeV, but the representation of polarization becomes increasingly unsatisfactory as the energy increases, especially at forward angles. The increasing importance of meson production and relativistic effects may account for the change in conventional optical model systematics in the 400–500 MeV range. Using the fits to the 200-, 300-, and 400-MeV data, we derived an average geometry potential shown in Table II. With the average geometry systematics, the data were again fitted by varying the potential strengths. Results are shown in Table II and graphically in Figs. 15 and

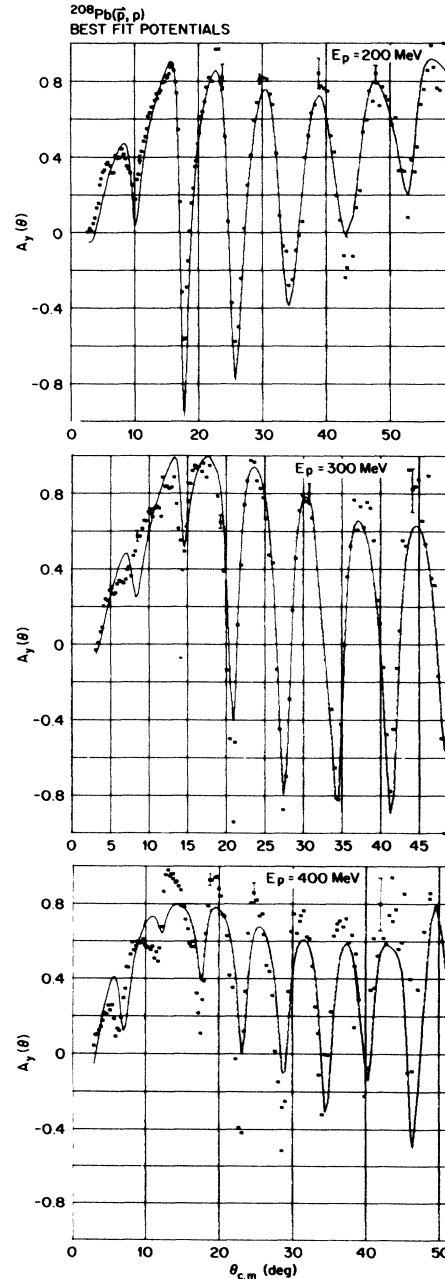


FIG. 14. Measured and calculated analyzing powers for elastic scattering of 200-, 300-, and 400-MeV polarized protons for ^{208}Pb . The data are from Ref. 5.

16. Parameters at 334 meV were obtained from a best fit to the data and by using the average geometry parameters deduced from the 200, 300, and 400 MeV fits and allowing the potentials to vary to provide a fit to the data. The 334 MeV data set is much smaller than those at 200–400 MeV and therefore the parameters obtained at 334 MeV are more uncertain than the others. An indication of this is the fact that the average geometry value (Table I) of W at 334 MeV is slightly lower than it is at 300 MeV.

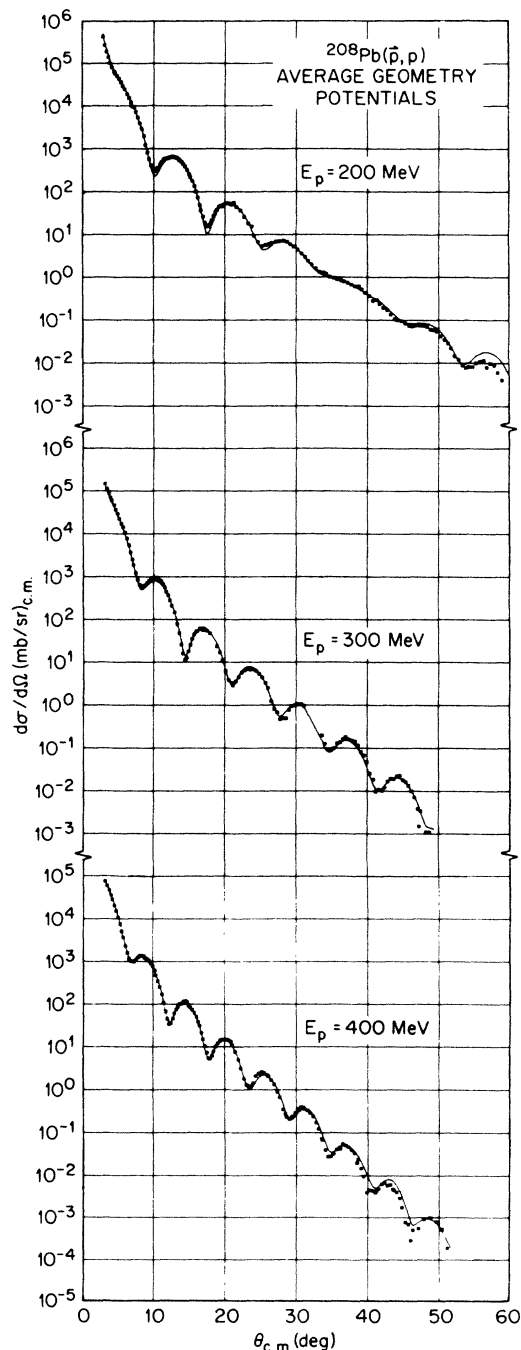


FIG. 15. Same as Fig. 13 except the calculations shown are those using the average geometry potential discussed in the text.

Nevertheless, as will be discussed below, DWBA calculations using the 334 MeV average geometry parameters provide good agreement with the data for well-known low lying states in ^{208}Pb .

Prior to the present analysis, the only optical model parameters available for this energy region were those deduced from a study of elastic scattering of 80–185 MeV protons.⁹ As is shown in Figs. 17 and 18, use of the parameters we have deduced from the higher energy data provides a better description of the elastic scattering of 200-MeV protons than the parameters extrapolated from the work of Ref. 8.

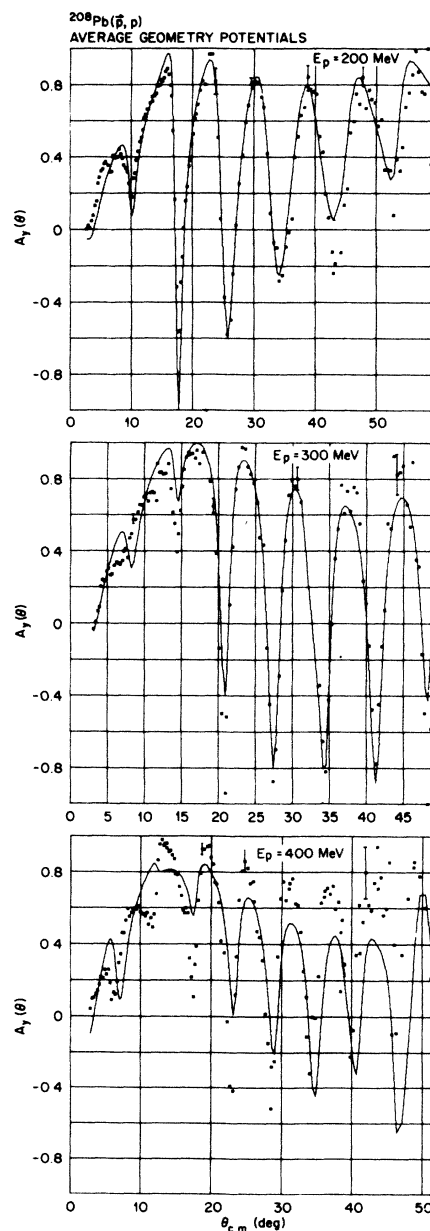


FIG. 16. Same as Fig. 14 except the calculations shown are those using the average geometry potential described in the text.

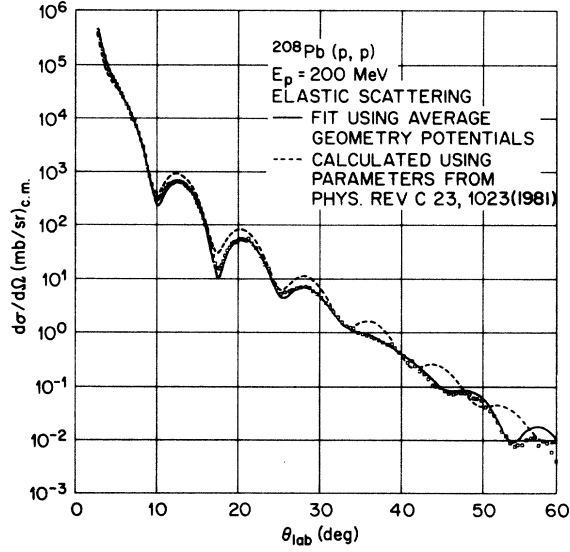


FIG. 17. Measured and calculated differential cross sections for elastic scattering of 200-MeV protons from ^{208}Pb . The data are from Ref. 5. The solid curve is from the DWBA calculation as described in the text using the average geometry potential deduced in the present work. The dashed curve is from the same calculation but using optical model potentials from Ref. 9.

B. Inelastic scattering

Analysis of the inelastic scattering cross sections and analyzing powers was made using the program ECIS.¹⁰ Calculations were performed using first order vibrational model couplings to 2^+ , 3^- , and 4^+ excited states.

For normal-parity excitations having $L \geq 2$, the resulting transition potentials have the radial form

$$U_{\text{tr}}(r) = \beta_L R \frac{dU(r)}{dr}, \quad (2)$$

where $\beta_L R$ is the deformation parameter to be determined from the data. All potential strengths in Table II (V_R , V_I , V_{so} , V_{iso} , and V_C) were allowed to be deformed but deformation lengths, $\beta_i R_i$, were generally taken to be equal except for the spin-orbit deformation lengths as discussed below.

Following the usual procedure, we extract the value of $\beta_L R$ by normalization of the calculated angular distribution to that measured:

$$(\beta_L R)^2 = (d\sigma/d\Omega)_{\text{measured}} / (d\sigma/d\Omega)_{\text{DWBA}}. \quad (3)$$

If β_L is assumed to be proportional to the mass multipole moment for a uniform distribution, then

$$(\beta_L R^L)^2 = B(EL) \left[\frac{4\pi}{3Z} \right]^2. \quad (4)$$

It has to be recognized that β_L in Eq. (3) refers to the deformation of the optical potential, while that in Eq. (4) is the deformation of the nuclear charge distribution. These two are not necessarily the same, which gives rise to uncertainties in comparing excitation strengths obtained by electromagnetic interactions and inelastic scattering of

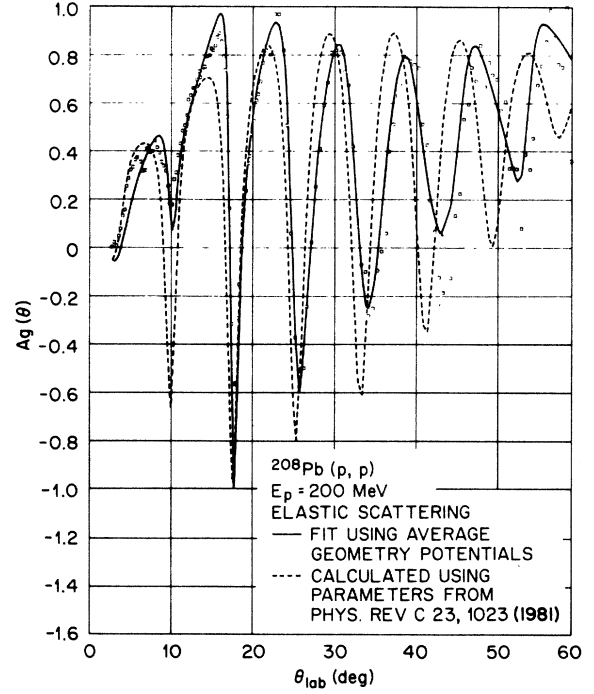


FIG. 18. Same as Fig. 17 except for analyzing powers.

nuclear projectiles. For giant resonances it is customary to express the deformation length in terms of the EWSR strength as

$$(\beta_L R)^2 = \frac{2\pi\hbar^2}{3m} \frac{L(2L+1)}{A} \frac{1}{E}. \quad (5)$$

Thus, for 100% of the EWSR located at energy E (MeV),

$$(\beta_L R)^2 \approx \frac{88}{AE} L(2L+1). \quad (6)$$

V. RESULTS AND DISCUSSION

A. Low-lying states

The calculated angular distributions for the 2^+ , 3^- , and 4^+ low-lying states shown in Fig. 7 are in agreement with the measured cross sections. The values of $\beta_L R$ shown in the figure were determined by normalization of the calculation to the data. Table III gives the value of the $B(EL)$ extracted from the best fit to the data (following the procedure described in Sec. IV) and the value of $B(EL)$ from the Nuclear Data Sheets.¹¹ Also shown is the $\beta_L R$ value obtained¹² for the same states through inelastic scattering of 800-MeV protons. The agreement of our results with those at 800 MeV and with the adopted values for the transition rate is excellent. The calculation for the $L=4$ transfer does not fit the data for the 4.323-MeV state near 5 deg. We believe that the data are too high in this region due to the fact that the cross section for the much stronger 4.086-MeV, 2^+ state reaches a maximum at $\sim 5-6$ deg; and even with 70-keV energy resolution, we could not completely separate the two peaks. We there-

TABLE III. Transition rates for low-lying states.

E_{level}^a (MeV)	J^π	$\beta_L R_{\text{this expt.}}$	$\beta_L R^b$	$B(EL)_{\text{this expt.}}^{\dagger}$ ($e^2 b^2$)	$B(EL)_{\text{adopted}}^{\dagger a}$ ($e^2 b^2$)
2.614	3^-	$0.83^{\pm 4}$	0.825	$0.67^{\pm 6}$	$0.611^{\pm 2}$
4.0854	2^+	$0.42^{\pm 4}$	0.466	$0.33^{\pm 1}$	$0.318^{\pm 16}$
4.3232	4^+	$0.48^{\pm 4}$	0.546	$0.12^{\pm 1}$	$0.155^{\pm 11}$

^aReference 11.^bReference 12.

fore discount the poor calculational agreement to the 4.323-MeV state near 5–6 deg.

The excellent agreement between the calculations and our data shows that when adequate elastic scattering data are available and a careful and systematic analysis of that data is performed, the DWBA provides an excellent description of both the shape and magnitude of the inelastic scattering to collective states by medium energy protons. There is little difference between the calculations using βR spin orbit equal to that for the real potential or for the case where βR spin orbit equals 0.75 of that for the real potential. There is a slight improvement in the comparison to the data in the valley of the angular distribution for the 3^- state and in the second maximum for the 2^+ state when the reduced βR spin-orbit value is used.

The use of the optical model parameters deduced in the present work in DWBA calculations for low-lying states also provides much better results than obtained with the use of the parameters suggested in Ref. 9. This is illustrated in Fig. 19 which shows the measured angular distribution for excitation of the 2.613 MeV, 3^- level in ^{208}Pb using 200-MeV protons.¹³ Using the same value of βR as deduced from the fit to our 334-MeV data, the calculation using the parameters from Ref. 9 overestimates the data

by $\sim 50\%$. However, use of the optical model parameters deduced in this work provides excellent agreement with the 200-MeV data.

As noted earlier, the $B(EL)$ values reported in Ref. 4 for the states listed in Table III are all low by a factor of about 2 when compared to the values from the present work, the 800 MeV work of Ref. 12, and the accepted values. As is shown in Ref. 13, the measured cross sections in Ref. 4 are low by a factor of 2 for the elastic scattering and inelastic scattering to the 2.613 MeV state.

The DWBA calculation provides a reasonable reproduction of the measured analyzing power for both the 2.613-MeV, 3^- , and 4.086-MeV, 2^+ states as seen in Fig. 8. The statistics for the 4.323-MeV, 4^+ state are too poor to allow extraction of the analyzing power. The DWBA calculation of the analyzing power agrees better with the data when the value of the spin-orbit deformation length is set equal to three-fourths of the real potential value rather than equal to the real potential value. However, we do not believe our analyzing power results are of sufficient accuracy to allow a firm conclusion to be reached.

B. Giant resonances

The change in the character of the giant resonance peak structure with changing angle as seen in the spectra of Fig. 4, agrees well with the calculated inelastic angular distributions for various angular momentum transfers as shown in Figs. 9–12. As noted previously, the 2.25-deg spectrum is dominated by excitation of the GDR located at 13.6 MeV. At forward angles excitation of the GDR proceeds almost entirely via Coulomb excitation, so that the cross section drops rapidly as the angle of observation is increased. One can see in Fig. 4 that with increasing angle the 13.6-MeV peak becomes smaller relative to the size of the 10.6-MeV GQR peak. The differential cross sections for the 13.6-MeV peak are plotted in Fig. 11 along with calculations of the cross section for excitation of the GDR and GMR. The calculation for the isovector dipole resonance includes both Coulomb and nuclear excitation, however, Coulomb excitation is dominant for angles smaller than about 7 deg. The monopole calculation follows version II of the prescription of Satchler.¹⁴ The computer code DWUCK was used for the calculations of the GMR and GDR angular distributions. While calculation of the Coulomb excitation cross section is well understood, the magnitude of the calculated nuclear excitation for the isovector GDR is dependent upon the value of the (t-t) term in the proton-nucleus optical potential.¹⁵ This term is very poorly determined for medium energy proton

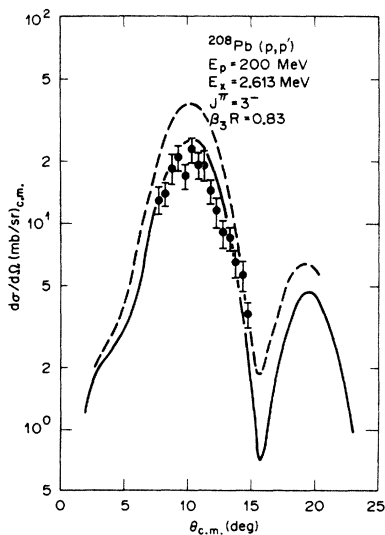


FIG. 19. Measured and calculated differential cross sections for excitation of the 2.613-MeV, 3^- state in ^{208}Pb by inelastic scattering of 200-MeV protons. The solid and dashed calculated curves have the same meaning as in Fig. 17. The data are from Ref. 13.

tons. We have used a value of -2.71 MeV based on the relation $V_1 = 59[1 - 0.18 \ln(E_p)]$ suggested by Nadasen *et al.*⁹ from studies at lower energies. In addition, we cannot test the validity of the GMR cross section calculation outside of using the monopole data itself. The best test of the model has come from GMR cross sections extracted from small angle inelastic scattering of alpha particles¹⁶ and helium-3's where the GMR cross section is maximized. In these cases, the monopole model provided a good description of the cross section.

It is with these qualifications that we interpret the angular distribution of the 13.6-MeV peak shown in Fig. 11. At the four most forward angles of measurement, the cross section agrees very well with the calculation for Coulomb excitation of the GDR under the assumption that 100% of the GDR EWSR is depleted in the peak. However, the measured cross section does not continue to fall as would be expected from the $L = 1$ calculation (solid curve), but rises to a maximum at ~ 6 deg then falls off smoothly. This behavior indicates the existence of a second excitation at the same energy, in good agreement with the known existence¹ of the GMR at 13.9 MeV. The maximum in the experimental angular distribution at ~ 6 deg occurs at the same angle as is calculated for the maximum of the $L = 0$ angular distribution. The sum of the $L = 0$ and $L = 1$ calculations does not provide enough cross section to agree with the data. Considering the uncertainties in the calculations, particularly in the nuclear part of the GDR calculation, such a discrepancy is not surprising. We conclude that the 13.6-MeV peak consists of nearly all GDR excitation (via Coulomb excitation) at the smallest angles and becomes a mixture in undetermined ratio of the GDR and GMR at larger angles.

The 2.25- and 3.24-deg spectra do not show the presence of any peaks above the GDR to an excitation energy of 25 MeV. This observation is in disagreement with a previous measurement⁴ of ^{208}Pb giant resonance spectra using 201-MeV protons. In that measurement, for $\theta_{\text{lab}} = 5$ deg, a compact peak was observed at 21.5 MeV of excitation energy. The authors of Ref. 4 interpret the 21.5-MeV peak as arising from the excitation of both an isovector quadrupole resonance and an isoscalar dipole resonance. The data from other inelastic proton scattering measurements¹³ on ^{208}Pb at 200 MeV which cover an excitation energy range from 0 to 40 MeV do not exhibit such a peak, but the smallest angle of observation in those measurements was 6 deg.

For angles of observation between 4.25 and 8.25 deg the spectra in Fig. 4 are dominated by a peak located at 10.6 MeV and by several narrower states located between the energies of 7 and 10 MeV. Within the accuracy of our measurements the narrow states all have a width of ~ 400 keV. Fitting the narrow peaks as shown in Fig. 4 and constraining the peak at 13.6 MeV to have a width determined by previous measurements of the GDR and GMR resonances leads to a width of 2.0 MeV for the 10.6-MeV peak.

The measured cross sections for the 10.6-MeV peak and for the six narrow peaks are plotted in Figs. 9 and 10, respectively, along with the calculated angular distribution for the L transfer that best fits the experimental data.

To deduce a value for the deformation length, βR , from which a value for the EWSR depletion is obtained, the calculations were normalized to the data at the first maximum of the angular distribution. The calculated curve in Fig. 9 is for an $L = 2$ transfer, and agrees very well with the shape of the experimental angular distribution. It is clear that the 10.6-MeV, 2.0-MeV wide peak arises from excitation of the GQR. Our results show that $70\% \pm 14\%$ of the $L = 2$, $T = 0$, EWSR is depleted in the peak. This result is in clear disagreement with the value of $24 \pm 3\%$ reported in Ref. 4 for the 201 MeV (p,p') reaction in ^{208}Pb . The excellent agreement between our measured cross sections for low-lying states having known spin, parity, and transition rate and the DWBA calculation provide confidence that our measurements of the EWSR depletions in the $L > 0$ isoscalar resonances are accurate. The DWBA calculation also provides a generally good description of the analyzing power of the GQR, although, the large minimum in the calculation at about 10 deg is not observed in the data.

Figure 10 shows the measured cross sections for the narrow peaks observed in the spectra between about 7 and 10 MeV. In several previous inelastic hadron scattering measurements, peaks have been observed at ~ 8.9 and 9.4 MeV. For example, the authors of Ref. 4 report the observation of a 1-MeV wide peak at 9.0 MeV which has an $L = 2$ angular distribution and a peak at 9.3 MeV which has an $L = 3$ distribution. The angular distribution of the 9.34-MeV peak in our data has a very clear $L = 2$ angular distribution in disagreement with the work of Ref. 4. Additional peaks in this excitation energy range have been reported¹⁷ in some previous hadron experiments. The narrow peaks observed in the present data were clearly seen at all angles of observation and their kinematic behavior rules out light contaminants on the target as the source of the peaks. It is to be noted that the width of the peaks is considerably broader than our 70-keV resolution.

The solid curves in Fig. 10 are from the DWBA calculation for the L transfer that best fits the data and agreement is excellent with the experimental angular distributions. From these comparisons we find that four of the states have spin and parity 2^+ , one has 3^- , and one has 4^+ . The sum of the $L = 2$ strength found in these states is $\sim 20\%$. This strength when added to the 70% found in the major GQR peak at 10.6 MeV, accounts for $90\% \pm 15\%$ of the $L = 2$, $T = 0$ EWSR. From previous measurements,¹⁸ and from our own results, we know that $\sim 15\%$ of the isoscalar quadrupole strength is found in states located below 7 MeV. Thus, within uncertainties we can account for all of the $L = 2$, $T = 0$, EWSR in ^{208}Pb .

From Fig. 4 it is seen that the character of the giant resonance spectra changes rather dramatically at ~ 9 deg. While the spectra at 4.25–8.25 deg can be well reproduced by use of the GQR and GDR or GMR peaks, such is not the case at the larger angles. As shown in Fig. 5, we have introduced a third peak located at 12.0 MeV, with a width of 2.4 MeV to fit the spectra. The measured cross sections for the 12-MeV peak are shown in Fig. 12. The uncertainties are large and include the considerable uncertainty of the peak stripping process. The solid and

dashed curves are DWBA calculations for $L=4$ and $L=2$ transfer, respectively, where the calculated cross section is normalized to the data. In spite of the large uncertainties in the data, the measured cross sections are clearly better described by the $L=4$ calculation than by that for $L=2$. We deduce from the data that $\sim 9\%$ of the $T=0$, $L=4$, EWSR is depleted in the 12.0-MeV peak. These results are in agreement with our previous observation⁸ of hexadecapole strength at the same position using 200-MeV protons.

A summary of the energy and widths of peaks extracted from our data between 7 and 25 MeV and the deduced angular momentum transfer and EWSR depletion for each peak are given in Table I.

VI. CONCLUSIONS

We have presented the results of measurements of the excitation of giant resonances in ^{208}Pb using inelastic scattering of 334-MeV protons. The data were obtained with an energy resolution of ~ 70 keV. We have also presented results for elastic scattering and for inelastic scattering to several well-known low-lying states.

We have used previously measured elastic scattering data⁵ for 200-, 300-, and 400-MeV protons on ^{208}Pb to provide input for a systematic optical model analysis. From this analysis we deduced an average geometry potential which provides an excellent fit to the elastic data at each of the three energies. Using that average potential we were able to obtain a good fit to our 334-MeV elastic scattering data.

Calculations of the inelastic scattering to low-lying states using the parameters (as listed in Table II) from our elastic scattering analysis provide good agreement with the measured angular distributions for three low-lying states in ^{208}Pb . The $B(EL)$ values deduced from comparison of the measured and calculated angular distributions agree with accepted values.¹¹ This fact establishes credibility in the use of the DWBA collective model calculation for extraction of the sum rule strength in giant resonances excited by medium energy protons. From our comparisons with the DWBA calculations we conclude that the DWBA collective model approach provides agreement with medium energy proton inelastic scattering data and can be used confidently to extract transition rates and EWSR values. Furthermore, we have shown elsewhere¹⁹ that the DWBA provides agreement with inelastic proton scattering excitation of the 2.613-MeV, 3^- state in ^{208}Pb at energies from ~ 60 –800 MeV. These results are in disagreement with the measurements of Ref. 4.

The spectra in the giant resonance region ($E_x > 7$ MeV) show the presence of a variety of giant resonance multipolarities. At the smallest angles the spectra are dominated by Coulomb excitation of the giant dipole resonance and we find no evidence for excitation at small angles of

higher-lying giant resonances.

Contrary to results from inelastic electron scattering in which no localized giant quadrupole resonance strength was found, our results clearly show the existence of a GQR peak located at 10.6 MeV having a width of 2.0 MeV. We find several narrow peaks located at excitation energies below the GQR. While most of these peaks arise from excitation of 2^+ states, one peak comes from a 3^- excitation and one from a 4^+ excitation. We cannot provide a reason why the (e,e') measurements of Ref. 2 fail to observe a compact GQR peak. The energy resolution in our present measurements is comparable to that in the electron work. Furthermore, the angular distributions in the present measurements provide a very high degree of angular momentum selectivity, thus eliminating the possibility that the compact peak arises from nonquadrupole excitations. Our angular distribution for the 10.6-MeV peak agrees with both the DWBA calculated $L=2$ angular distribution and with the shape of the experimental angular distribution for the 4.086-MeV, 2^+ state. We find 70% of the $L=2$ EWSR strength to be depleted in the 10.6-MeV peak in contrast with the observation of 20–40 % in the same region in the electron scattering experiment and in the measurement of Ref. 4 with 201 MeV protons. Our results for the EWSR depleted in the GQR peak are consistent with those recently reported¹³ from the measurement of inelastic scattering of 200 MeV protons on ^{208}Pb . Including the five 2^+ states in the 7–9-MeV region of excitation and the known low-lying 2^+ states, we account for 100% of the $L=2$, $T=0$, EWSR strength in ^{208}Pb .

For scattering angles larger than approximately 9 deg we find clear evidence for the excitation of hexadecapole strength in the form of a peak located at 12.0 MeV having a width of 2.4 MeV. The angular distribution for the 12-MeV peak agrees very well with the calculated angular distribution for an $L=4$ excitation depleting $\sim 10\%$ of the EWSR. This result is in agreement with our earlier observation⁸ using 200-MeV proton inelastic scattering. The $L=4$ strength is interpreted as arising from excitation of the $2\hbar\omega$ portion of the hexadecapole giant resonance. An indication of the excitation of the now well-established giant octupole ($3\hbar\omega$) resonance was seen. However, we cannot provide a proper measurement for this resonance because our spectra are limited to 25 MeV of excitation energy.

ACKNOWLEDGMENTS

This work was supported by Oak Ridge National Laboratory, operated by Martin Marietta Energy Systems, Inc. under Contract DE-AC05-84OR21400 with the U.S. Department of Energy. The University of Oregon and Oregon State University participants were supported in part by grants from the National Science Foundation.

- ¹F. E. Bertrand, Nucl. Phys. **A354**, 129c (1981).
- ²G. Kühner, D. Meuer, S. Müller, A. Richter, E. Spamer, and O. Titze, Phys. Lett. **104B**, 189 (1981).
- ³H. P. Morsch, P. Decowski, and W. Benenson, Nucl. Phys. **A297**, 317 (1978).
- ⁴C. Djalali, N. Marty, M. Morlet, and A. Willis, Nucl. Phys. **A380**, 42 (1982).
- ⁵D. Hutcheon, (unpublished).
- ⁶R. A. Arndt, R. H. Hackman, and L. D. Roper, Phys. Rev. C **9**, 555 (1974); R. A. Arndt, Virginia Polytechnic Institute N-N Program.
- ⁷B. L. Berman and S. C. Fultz, Rev. Mod. Phys. **47**, 713 (1975).
- ⁸J. R. Tinsley, D. K. McDaniels, J. Lisantti, L. W. Swenson, R. Liljestrand, D. M. Drake, F. E. Bertrand, E. E. Gross, D. J. Horen, and T. P. Sjoreen, Phys. Rev. C **28**, 1417 (1983).
- ⁹A. Nadasen, P. Schwandt, P. P. Singh, W. W. Jacobs, A. D. Bacher, P. T. Debevec, M. D. Kaitchuck, and J. T. Meek, Phys. Rev. C **23**, 1023 (1981).
- ¹⁰J. Raynal, private communication.
- ¹¹M. J. Martin, Nucl. Data Sheets **47**, 797 (1986).
- ¹²M. M. Gazzaly, N. M. Hintz, G. S. Kyle, R. K. Owen, G. W. Hoffman, M. Barlett, and G. Blanpied, Phys. Rev. C **24**, 408 (1982).
- ¹³D. K. McDaniels, J. R. Tinsley, J. Lisantti, D. M. Drake, I. Bergqvist, L. W. Swenson, F. E. Bertrand, E. E. Gross, D. J. Horen, and T. P. Sjoreen, Phys. Rev. C (in press).
- ¹⁴G. R. Satchler, Part. Nuclei **5**, 105 (1973).
- ¹⁵G. R. Satchler, Nucl. Phys. **A195**, 1 (1972).
- ¹⁶D. H. Youngblood, C. M. Rozsa, J. M. Moss, D. R. Brown, and J. D. Bronson, Phys. Rev. Lett. **39**, 1188 (1977); M. Buerd, C. Bonhomme, D. Lebrun, P. Martin, J. Chauvin, G. Duhanel, G. Perrin, and P. de Saintignon, Phys. Lett. **84B**, 305 (1979).
- ¹⁷For example see: H. P. Morsch, P. Decowski, M. Rogge, P. Turek, L. Zemlo, S. A. Martin, G. P. A. Berg, W. Hürlimann, J. Meissburger, and J. G. M. Römer, Phys. Rev. C **28**, 1947 (1983); H. P. Morsch, P. Decowski, and W. Benenson, Nucl. Phys. **A297**, 317 (1978).
- ¹⁸M. B. Lewis, F. E. Bertrand, and C. B. Fulmer, Phys. Rev. C **7**, 1966 (1973).
- ¹⁹D. K. McDaniels, J. Lisantti, J. Tinsley, I. Bergqvist, L. W. Swenson, F. E. Bertrand, E. E. Gross, and D. J. Horen, Phys. Lett. **162B**, 277 (1985).